DOI: 10.1002/chem.201001053

Ultrasensitive SERS Detection of TNT by Imprinting Molecular Recognition Using a New Type of Stable Substrate**

Liangbao Yang,[a] Liang Ma,[b] Guangyu Chen,[b] Jinhuai Liu,*[a] and Zhong-Qun Tian[c]

Abstract: We report herein a method for the ultra-trace detection of TNT on *p*-aminothiophenol-functionalized silver nanoparticles coated on silver molybdate nanowires based on surface-enhanced Raman scattering (SERS). The method relies on π-donor–acceptor interactions between the π-acceptor TNT and the π-donor *p*,*p*′-dimercaptoazobenzene (DMAB), with the latter serving to cross-link the silver nanoparticles deposited on the silver molybdate nanowires. This system presents optimal imprint molecule contours, with the DMAB forming imprint molecule sites that constitute SERS "hot spots". Anchoring of the TNT analyte at these sites leads to a pronounced intensification of its Raman emission. We demonstrate that TNT concentrations as low as 10^{-12} M can be accurately detected using the described SERS assay. Most impressively, acting as a new type of SERS substrate, the silver/silver molybdate nanowires complex can yield new silver nanoparticles during the detection process, which makes the Raman signals very stable. A detailed mechanism for the observed SERS intensity change is discussed. Our experiments show that TNT can be detected quickly and accurately with ultra-high sensitivity, selectivity, reusability, and stability. The results reported herein may not only lead to many applications in SERS techniques, but might also form the basis of a new concept for a molecular imprinting strategy.

Keywords: imprinting · molecular recognition · Raman spectroscopy · silver · TNT

Introduction

Synthetic functional host molecules, such as calixarenes (CXs),[1–6] cyclodextrins (CDs),[7–11] and viologen dications (VGD),[12–15] that are capable of binding target molecules, have attracted considerable research interest in relation to SERS. The affinity of a metal surface can be increased by its functionalization with host molecules or cavitands. To accomplish the objective of ultra-trace detection by SERS analysis, the host is of the utmost importance. The host has to possess several features: 1) a strong affinity for both the surface of the metal nanoparticles and the target molecules, 2) adoption of good self-assembly organization at the metal–liquid interface with optimal imprint molecule contours, 3) high selectivity, 4) imprinting of molecular recognition sites, 5) low band overlap with the Raman features of the target molecule, and 6) bifunctionality, to induce "hot-spot" formation, the approach of the target molecule near which leads to enormous electromagnetic intensification. We believe that the molecule *p*-aminothiophenol meets these requirements.

2,4,6-Trinitrotoluene (TNT) is a manmade explosive that is deployed in the preparation of landmines for military and terrorist activities.[16,17] It is used in underwater blasting and also has industrial applications. TNT is regarded as a priority pollutant with top recommendation for removal from contaminated sites since it is toxic to living forms. TNT can be absorbed through the skin and persons who are exposed to it over a prolonged period tend to experience anemia and abnormal liver function. It is also regarded as a possible human carcinogen. Accidental release of TNT has contami-

[a] L. Yang, J. Liu
Institute of Intelligent Machines, Chinese Academy of Sciences
Hefei 230031 (P.R. China)
Fax: (+86) 551-5592420
E-mail: jhliu@iim.ac.cn

[b] L. Ma, G. Chen
Department of Chemistry
University of Science and Technology of China
Hefei, 230026 (P. R. China)

[c] Prof. Z.-Q. Tian
State Key Laboratory of Physical Chemistry of Solid Surfaces
College of Chemistry and Chemical Engineering
Xiamen University, Xiamen 361005 (P. R. China)

[**] SERS = surface-enhanced Raman scattering.

Supporting information for this article is available on the WWW under http://dx.doi.org/10.1002/chem.201001053.

nated groundwater and soil at numerous munitions manufacturing sites.[18] Recently, global security concerns have also dictated a need for the detection of hidden explosive devices in war zones and transportation hubs. Detection of TNT is important for various disciplines, including humanitarian demining, remediation of explosives waste sites, homeland security, and forensic applications. Current technology for the identification of TNT requires a great deal of time and effort, being reliant upon the employment of either a cumbersome and expensive gas chromatograph coupled to a mass spectrometer, ion mobility spectrometry, or neutron activation analysis.[19,20] These methods are too slow from the perspective of the day-to-day life needs for on-the-spot detection. As a result, it is important to develop an ultrasensitive, cost-effective probe that can provide real-time determination of TNT levels in the environment.

The phenomenon of SERS is generally explained in terms of a combination of an electromagnetic (EM) mechanism describing the surface electron movement in the substrate and a chemical mechanism related to charge transfer (CT) between the substrate and the analyte molecules.[21] The level of detection specificity is a very important feature of SERS, which can be achieved by controlling the chemistry around the metal surface. By incorporating a specific chemical moiety on the relevant surface, one can target the detection of a single species present in a complex sample mixture. In a recent study, Willner and co-workers demonstrated the use of thioaniline-modified Au NPs as building units to construct an electropolymerized bis-aniline cross-linked Au NPs composite on Au electrodes. The cross-linked Au NPs matrix associated with the electrode was used for the electrochemical[22] and surface plasmon resonance detection[23] of TNT. We report here for the first time *p*-aminothiophenol-modified silver nanoparticles coated on silver molybdate nanowires (SMNs) as a surface-based, inexpensive, and ultrasensitive SERS probe that allows highly sensitive and selective screening of TNT in aqueous solution. We introduce a very simple new method for the imprinting of molecular recognition sites based on a catalytic coupling reaction to selectively produce a new surface species, *p*,*p*′-dimercaptoazobenzene (DMAB), on functional silver NPs on SMNs. We have developed a new concept for the imprinting method in this study. Our previous studies used traditional imprinting procedures in organic or inorganic polymer matrices and focused on miniaturizing the polymer components into small beads, such as polymer nanowires,[24] silica nanotubes,[25] and core–shell silica particles.[26] The new imprinting approach described here may be considered as "imprinting at the nanoscale". In this system, the functionalized Ag NPs act as the matrices, *p*-aminothiophenol (PATP) is used as functional monomer, and DMAB acts as a cross-linking agent for the photonic catalytic coupling imprinting process. To the best of our knowledge, this is the first instance of the utilization of PATP without functionalization as a host molecule with the subsequent imprinting of molecular recognition sites for TNT on cross-linked silver NPs. Our method relies on the fact that the imprinting of molecular recognition sites can generate "hot spots" through aggregation on the *p*-aminothiophenol-modified silver NPs surface. Our results demonstrate the potential for broad application of this type of nanotechnology in practical applications, for example in pesticide detection systems.

In reality, the enhancement properties of an SERS-active surface are highly dependent upon its method of preparation and therefore its detailed nanostructure. To apply SERS in routine, on-line studies for analytical purposes, the substrate of Ag nanoparticles on SMNs needs to be stable, easily and reproducibly prepared, and relatively inexpensive.

Results and Discussion

Interactions between PATP and TNT: Utilization of the natural tendency of some molecules to self-assemble through various noncovalent interactions has been extensively explored in the fabrication of biological and chemical sensors. In this study, we have developed a very simple approach to assemble TNT molecules on the functional silver and SMNs (Ag-SMNs) complex. The SMNs are covered with silver nanoparticles, which are first modified with PATP, resulting in an amino monolayer on their surface. The assembly of TNT molecules is based on the very strong acid–base pairing interaction between the electron-rich amino group of PATP and the electron-deficient aromatic ring of TNT, which is similar to the affinity binding of TNT molecules to electron-rich 3-aminopropyltriethoxysilane (APTS)-modified alumnia pore walls.[24] The interaction between TNT and PATP has been demonstrated by measurement of UV/Vis absorbance spectra. Figure 1 shows the evolution of the UV/Vis spectra of a TNT solution containing increasing amounts of PATP. The new absorption bands appear at about 525 nm, and strengthen continuously with increasing amount of PATP in the TNT solution, as indicated in

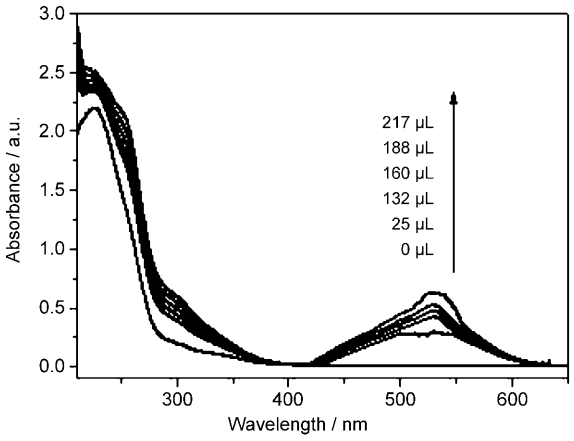

Figure 1. Acid–base pairing interaction between TNT and PATP molecules: the evolution of UV/Vis absorbance spectra with the addition of different volumes (0, 25, 132, 160, 188, 217 μL) of PATP to 2.5 mL of 0.1 mM TNT solution (solvent: ethanol/acetonitrile, 8:2). PATP: 0.1 mM.

Figure 1. The concentration of TNT was 0.1 mM, and the concentrations of PATP corresponded to 0, 1×10^{-5}, 5×10^{-5}, 6×10^{-5}, 7×10^{-5}, and 8×10^{-5} mM. It can be seen that the color of the solution gradually changes from colorless to red. This observation of visible absorption clearly demonstrates that there is a strong intermolecular interaction between the electron-deficient aromatic ring of TNT and the electron-rich amino group of PATP in the solution system. The negative charge on the TNT anion is distributed throughout the molecule through resonance stabilization by the three electron-withdrawing nitro groups.[29] In this state, PATP has been demonstrated to be a zwitterion.[30] As illustrated in Scheme 1A, the anion–cation pair of TNT^- and

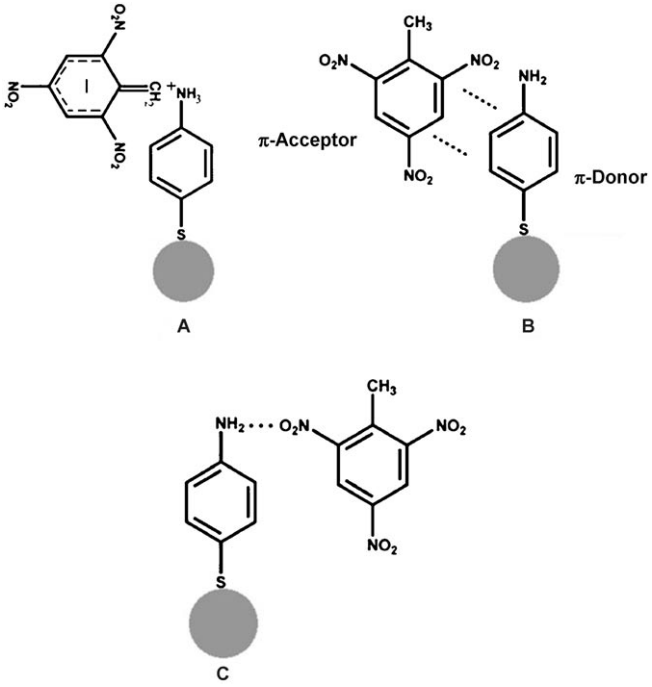

Scheme 1. Schematic representation of the possible interactions between TNT and PATP: A) through the anion–cation pair, B) π-donor–acceptor interactions, and C) possible hydrogen-bonding interaction.

NH_3^+ was formed in the present solution system. Scheme 1B depicts the formation of π-donor–acceptor interactions. It is known that PATP serves as a π-donor and that TNT serves as a π-acceptor, which clearly suggests the formation of a complex between PATP and TNT in solution based on π-donor–acceptor interactions.[23] In this situation, there may also be hydrogen bonding (as shown in Scheme 1C), besides the electrostatic interaction and π-donor–acceptor interactions.

When the PATP-modified Ag-SMNs complex is immersed into a solution of TNT, the strong complexing effects will drive the TNT molecules to assemble on the surface of the Ag-SMNs. The TNT assembly was carried out by simply immersing the PATP-modified Ag-SMNs complex into a 1 mM solution of TNT. Figure 2 (curve 3) shows the new visible absorbance at 525 nm, which clearly reveals that TNT can

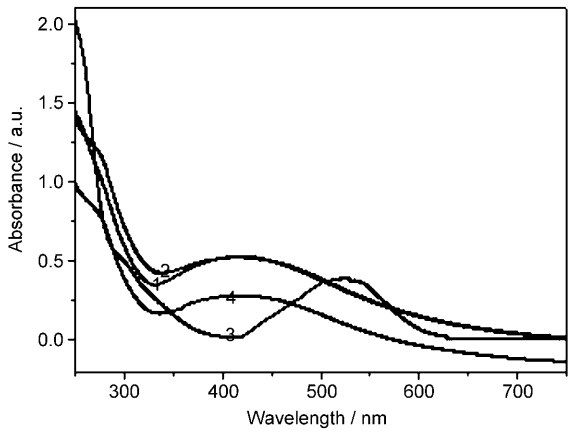

Figure 2. UV/Vis spectra of: 1) Ag-SMNs complex, 2) PATP-modified Ag-SMNs complex, 3) PATP-modified Ag-SMNs complex in the presence of TNT, and 4) PATP-modified Ag-SMNs complex in the presence of DNT.

be directed to the circumference of the surface of Ag-SMNs, where it is enriched through its interactions with the PATP molecules. Figure S2 A in the Supporting Information shows a TEM image of PATP-modified Ag-SMNs complex solution in the absence of TNT. When TNT was added to the PATP-modified Ag-SMNs complex solution, as shown in Figure S2 B in the Supporting Information, aggregations were formed, as was reported in a previous study.[21] This may be attributed to interactions between PATP and TNT as discussed above. Aggregation in the presence of TNT ions also results in a substantial shift in the plasmon band energy to longer wavelength (525 nm). Thus, the TEM data clearly show that TNT helps to generate "hot spots" through aggregation at the surface of the PATP-modified Ag-SMNs complex. We did not observe any visible band between 450 and 750 nm in the presence of DNT (Figure 2, curve 4). So, the results clearly demonstrate that DNT is not able to form an interaction complex, even at higher concentration. In the case of DNT, it is most probably possible to deprotonate at the methyl group. However, due to the lack of an $-NO_2$ group at the 6-position of the benzene ring, partial negative charge may not be distributed throughout the ring. Due to the lack of sufficient anionic charge, DNT may not form an interaction complex, which is similar to the finding that cysteine cannot form a Meisenheimer complex in the presence of DNT.[21]

The process of "imprinting at the nanoscale" and the formation of "hot spots" for TNT based on a catalytic coupling reaction of PATP: It is known that azobenzene compounds can be selectively formed from aniline and its substituted derivatives by environmentally friendly gold nanoparticle-catalyzed synthesis.[31] Aromatic amines can be catalytically oxidized to the corresponding azo compounds in the presence of silver or gold ions, gold or silver nanoparticles by light irradiation, or electrochemical anodic polarization in alkaline solutions.[31–35] On the basis of theoretical calcula-

tions combined with literature reports, Wu et al.[36] demonstrated that PATP molecules adsorbed on nanoscale rough surfaces of noble metals and nanoparticles undergo a catalytic coupling reaction to selectively produce a new surface species, *p*,*p*′-dimercaptoazobenzene (DMAB). No fundamentals were found in their cluster model calculations that matched the vibrational frequencies of 1142, 1391, and 1440 cm^{-1} observed in the SERS of PATP on rough electrodes and silver nanoparticles.[37–39] The peak positions of these intense SERS bands observed experimentally could not be reproduced by calculations on PATP interacting with various silver clusters. It was concluded that the experimentally observed bands do not arise directly from PATP adsorbed on silver surfaces.[36] Therefore, the observed phenomenon in SERS of PATP should be attributable to some new surface species, DMAB. In our study, we observed the same experimental phenomenon. The Raman spectrum of solid PATP (Figure 3, curve 1) is very different from that of

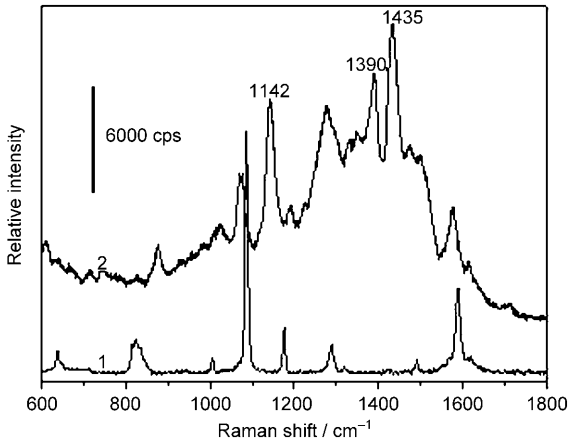

Figure 3. Raman and SERS spectrum of 1) solid PATP, 2) SERS spectrum of PATP-modified Ag-SMNs complex.

PATP-modified Ag-SMNs under light irradiation (Figure 3, curve 2). The peaks at 1142, 1390, and 1435 cm^{-1} observed in our SERS spectrum (Figure 3, curve 2) can be attributed to DMAB, which is produced by the catalytic coupling reaction of PATP on rough silver nanoparticle surfaces as a result of nanoparticle-assisted photonic catalytic oxidation. The outcome is different from that of the electrochemical process.[23]

The major steps involved in the imprinting synthesis and the formation of "hot spots" are shown in Scheme 2. In the

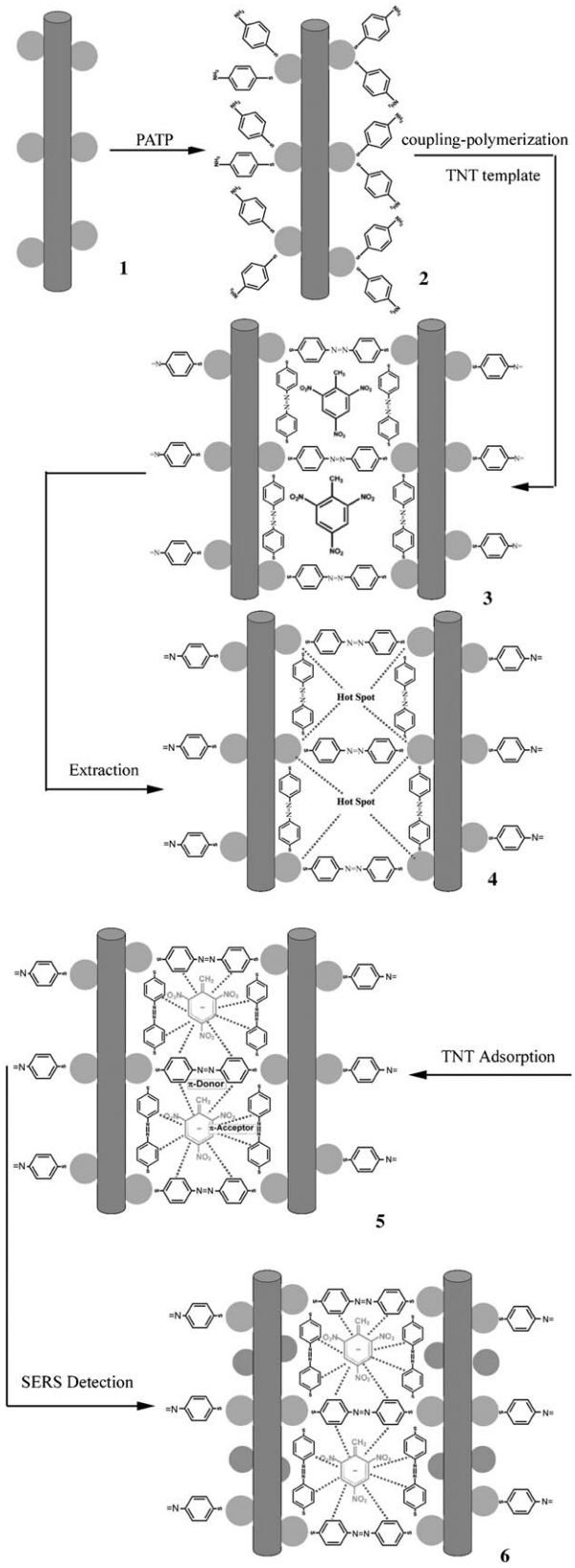

Scheme 2. Schematic illustration of the molecular imprinting of TNT and the formation of "hot spots" in Ag-SMNs complex. Ag-SMNs complex **1** was modified with PATP, leading to the PATP-Ag-SMNs complex **2**. The imprinted particles **3** were prepared through coupling polymerization in the presence of TNT templates and DMAB-Ag-SMNs complex. After removal of the templates, the particles **4** were obtained. The particles **5** could be formed through anchoring of TNT at the imprinted molecular recognition sites by donor–acceptor interactions. Under laser irradiation, more small Ag nanoparticles appeared on the surfaces of the particles (**6**).

first step, Ag-SMNs **1** synthesized in situ by the UV-irradiation method are chemically modified with PATP, which acts as a π-donor. The functionalized Ag-SMNs complex **2** was then subjected to a coupling polymerization reaction to yield the DMAB π-donor-bridged Ag-SMNs complex **3**. During the coupling polymerization, the π-donor–acceptor complex between TNT and the DMAB-modified Ag-SMNs is formed. The coupling polymerization is based on the results of our experiments (the Raman spectra in Figure 3) and the study of Wu.[36] The aim of the present study is to enhance the sensitivity of TNT analysis by modifying the surface of Ag nanoparticles with π-donor groups that would concentrate the TNT analyte through π-donor–acceptor interactions and by providing optimally arranged molecular contours. We also believe that the formed DMAB π-donor-bridged Ag-SMNs complex (**3**) and this π-donor–acceptor interaction help DMAB-modified Ag-SMNs complex to aggregate in the presence of TNT. As a result, an array of "hot spots" was formed, anchoring of the analyte at which would lead to a significant enhancement of Raman signal intensity. Subsequent removal of the TNT imprinting molecules by solvent extraction left molecular contours (**4**) with optimally positioned π-donor sites for subsequent association of the TNT analyte. Indeed, it was demonstrated in electrochemical sensors that the synergistic binding of TNT through π-donor–acceptor interactions and molecular contours improved its association constant.[22] Finally, when the SERS substrate with adsorbed TNT (**5**) was subjected to laser irradiation, the SMNs were covered with more freshly generated Ag nanoparticles with an average diameter of 15 nm (**6**) (see the smaller spheres in Figure 4D). As silver molybdate is a layered compound, these freshly generated Ag nanoparticles might shift to ideal locations because the laser beam is focused strongly on an extremely small object,[40,41] which is favorable with respect to the surface-enhanced factor.[42] At the same time, our experiments have demonstrated that the SERS substrate displays excellent stability (see Figure S1 in the Supporting Information).

Previously, we have used traditional imprinting procedures on organic or inorganic polymer matrices and have focused on miniaturizing the polymer sizes into small beads.[26] The new methodology described here may be termed "imprinting at the nanoscale". The Ag NPs act as a matrix, PATP and DMAB are used as the functional monomer and cross-linking agent, and the polymerization imprinting process occurs by photonic catalytic coupling.

In brief, significant enhancement of the Raman signal intensity is based on the formation of a multitude of "hot spots", which is evident from TEM images of DMAB-modified Ag-SMNs complex (see Figure S2 in the Supporting Information), optimal imprinted molecule contours, and more imprint molecule recognition sites.

Design, synthesis, and characterization of the new type of Ag-SMNs complex SERS substrate: Herein, a unique approach for preparing SERS substrates is proposed by utilizing silver molybdate as the raw material. Silver molybdate nanowires were synthesized on a large scale through a simple solution approach at room temperature. Silver nanoparticles were then obtained by using UV light to irradiate silver molybdate solution, whereby silver nanoparticles were deposited on the surface of silver molybdate nanowires in situ. X-ray diffraction patterns demonstrated the phase change before and after UV light irradiation (see the Supporting Information). To the best of our knowledge, such a solution synthesis of a silver and silver molybdate nanowires complex has not hitherto been described in the literature. The Ag-SMNs complex displayed ultrasensitivity in the SERS detection of TNT, which is similar to what was found for a SERS substrate of silver nanoparticles deposited on β-silver vanadate nanowires.[42]

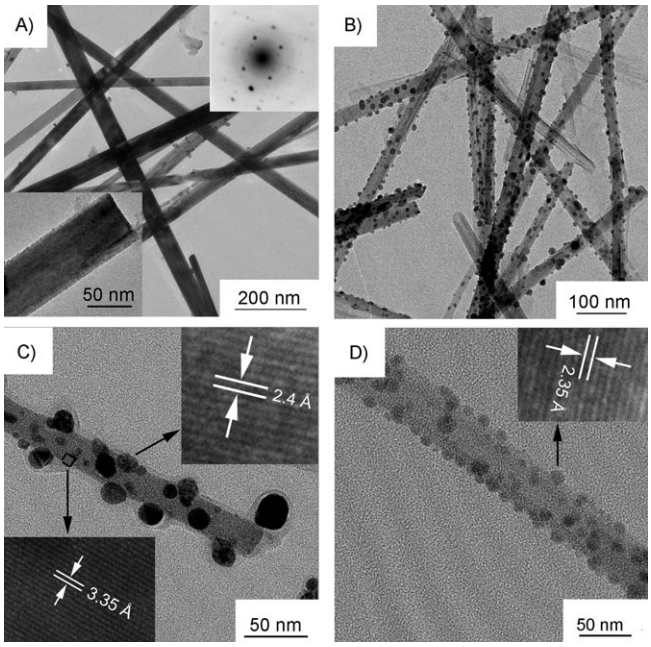

Figure 4. TEM images of A) SMNs and B) SMNs covered with Ag nanoparticles; the insets in A show an individual SMN and the electron-diffraction pattern; C) TEM image of an individual SMN covered with Ag nanoparticles, insets: crystal-lattice images of an individual Ag nanoparticle and the SMN; D) TEM image of an SMN covered with numerous Ag nanoparticles after laser irradiation, inset: crystal lattice image of an Ag nanoparticle.

In this study, a solution method has been employed to synthesize the SMNs. TEM images revealed that the SMNs were generally ultra-long with lengths up to several micrometers. When the reaction solution was simultaneously irradiated with UV light, freshly generated silver nanoparticles were deposited in situ. The TEM image in Figure 4A shows that the particles were rod-like with a diameter of about 50 nm, and it is also apparent that the surfaces of the crystals were smooth. The inset in Figure 4A shows the associated selected area electron diffraction (SAED) pattern recorded by focusing the incident electron beam on an individual nanowire and is indicative of the single-crystalline nature of the wire. We also carried out extensive investigations on more individual wires by means of electron diffrac-

tion (ED), the results of which confirmed that the as-synthesized sample was single-crystalline. Based on the XRD and electron-diffraction patterns, we concluded that the nanowires grew preferentially along the *c* axis. The TEM image in Figure 4B shows that the SMNs were almost completely covered with Ag nanoparticles with an average diameter of 16 nm. The high-resolution TEM image in Figure 4C shows that tiny nanoparticles with sizes of 10–25 nm were attached on the backbone of the SMNs. Interestingly, no silver nanoparticles were observed in isolation from the SMNs in the solution, indicating that Ag^+ reduction occurred only on the surface of the $Ag_6Mo_{10}O_{33}$ colloidal particles. This suggests that the $Ag_6Mo_{10}O_{33}$ colloidal particles act as excellent templates. From the insets in Figure 4C, Ag NP and SMN are seen to be single-crystalline, with their growth directions along the [111] and [022] axes, respectively. The crystal lattices of Ag and $Ag_6Mo_{10}O_{33}$ may be indexed to the (111) and (022) crystal planes, because the spacings of 0.24 nm and 0.335 nm correspond to the Ag (111) plane and the $Ag_6Mo_{10}O_{33}$ (022) plane respectively. Most interestingly, after exposure to laser irradiation for a longer time, more and more smaller spherical nanoparticles of about 12 nm in size appeared on the backbones of the $Ag_6Mo_{10}O_{33}$ nanowires (Figure 4D). At first, we supposed that the fresh nanoparticles may arise because the $Ag_6Mo_{10}O_{33}$ nanowires partially melt under laser irradiation and amorphous particles are formed following their destruction (the melting point of this compound is about 236 °C). An HRTEM image (inset in Figure 4D) of a nanoparticle clearly manifests its crystalline nature. The crystal lattice spacing proved these nanoparticles to be Ag crystals, with the growth direction along the [111] axis. Hence, our initial supposition was wrong. It is very important that this reaction system is a perfect laser-excited SERS substrate. Sanchez-Cortes and co-workers have demonstrated that Ag nanoparticles may be prepared by laser photoreduction.[43] The Raman signals in our experiments were found to be very stable, due to more and more freshly generated silver nanoparticles being deposited under the conditions of laser irradiation. Some of these nanoparticles are very near to one another, and these nanoparticles in close proximity can lead to plasmonic coupling, which results in huge local electromagnetic field enhancements in these confined junctions or SERS "hot spots". Our data clearly show that this kind of SERS substrate can lead to magnitude enhancement of the Raman signal (see below).

In addition, the imprinted DMAB-modified Ag-SMNs complex could be recycled by extracting the analyte TNT, and it displayed excellent stability (see Figure S1 in the Supporting Information). The imprinted DMAB-modified Ag-SMNs complex still operated after one month at room temperature, showing only about a 10% decrease in the TNT signal. The most important reason for this is that the Ag-SMNs complex can yield plenty of new silver nanoparticles to cover the SMNs under the laser irradiation (see Figure 4D and Figure S3 in the Supporting Information).

SERS study and limit of detection of TNT: Figure 5 shows the Raman spectrum of powdered TNT, and the SERS spectra obtained for the as-prepared DMAB-modified Ag-SMNs complex and 1 nM TNT upon addition to the DMAB-modified Ag-SMNs complex. We observed that the Raman vibration modes for Ag-SMNs are quite weak and show no band overlap with the Raman features of the target or host molecules (see Figure S4 in the Supporting Information). Addition of PATP to this Ag-SMNs complex suspension resulted in a new set of peaks (Figure 5, curve 1) at 1142, 1390, and 1435 cm^{-1}, corresponding to the new species DMAB.[36] Comparing curve 1 with curve 2, the SERS spectrum obtained for the particle (**6** in Scheme 2) was significantly different to that for PATP-modified Ag-SMNs alone with respect to both observed bands and relative intensities. There is, however, some overlap between the SERS spectra of PATP-modified Ag-SMNs and the particle (**6** in Scheme 2). As can be seen in curve 2 of Figure 5, the SERS spectrum of the particle (**6** in Scheme 2) comprises a mixture of both the DMAB-functionalized Ag-SMNs and the TNT bands, revealing strong spectral changes in both species. The SERS spectrum features several prominent TNT peaks. The peak at 1609 cm^{-1} is due to the C=C aromatic stretching vibration. The strong Raman band at 1359 cm^{-1} is due to the NO_2 symmetric stretching vibration and the weak band at 1532 cm^{-1} is due to the NO_2 asymmetric stretching vibration. All of these are due to TNT vibration.[21] Featureless spectra were obtained when solutions of TNT were added to the colloidal suspension in the absence of PATP functionalization (data not shown). On the contrary, when TNT solutions were added to the PATP-functionalized Ag-SMNs, intense Raman bands of TNT appeared. The observation of TNT features can only be attributed to the formation of a π-donor–acceptor complex with DMAB. The main bands of these spectra as well as their assignments are shown in Table 1.

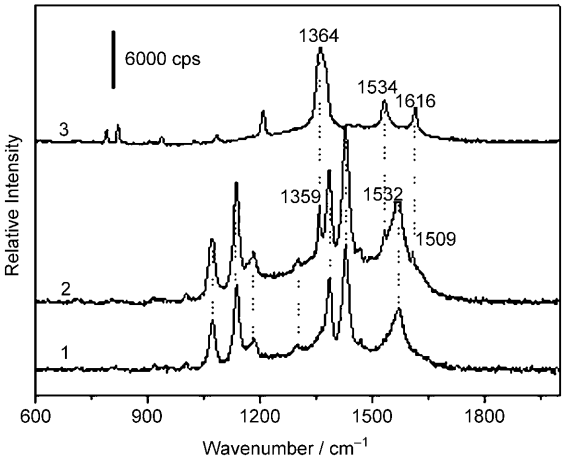

Figure 5. SERS spectra of 1) DMAB-modified Ag-SMNs complex, 2) DMAB-modified Ag-SMNs complex in the presence of TNT; 3) Raman spectrum of TNT in the solid state. Excitation at 514.5 nm; [PATP] = 10^{-6} M and [TNT] = 1 nM.

Table 1. Raman and SERS bands (cm^{-1}) and the band assignments for TNT, PATP, and DMAB within the wavenumber range of 1000–1650 cm^{-1}.

Raman of TNT	SERS of TNT	Assignments	Raman of PATP	SERS of PATP (DMAB)	Assignments
			1004	1025	$\alpha_{CCC}+\upsilon_{CC}$
			1085	1074	$\upsilon_{CC}+\upsilon_{CS}$
			1175	1185	$\beta_{C\text{-}H}$
1365	1359	$\nu_s(NO_2)$	1290	1278	υ_{CC}
1534	1532	$\nu_{as}(NO_2)$	1492	1478	$\beta_{C\text{-}H}+\upsilon_{CC}$
1616	1609	ν(C=C)	1591	1580	υ_{CC}
				1142	DMAB
				1390	DMAB
				1435	DMAB

To identify the optimum PATP concentration for the detection of TNT, SERS spectra of the particle (**6** in Scheme 2) were collected by varying the concentration of the π-donor PATP over the range from 10^{-4} to 10^{-9} M, while the TNT concentration was kept constant at 10^{-7} M. In Figure 6, the intensity of the TNT marker SERS band at

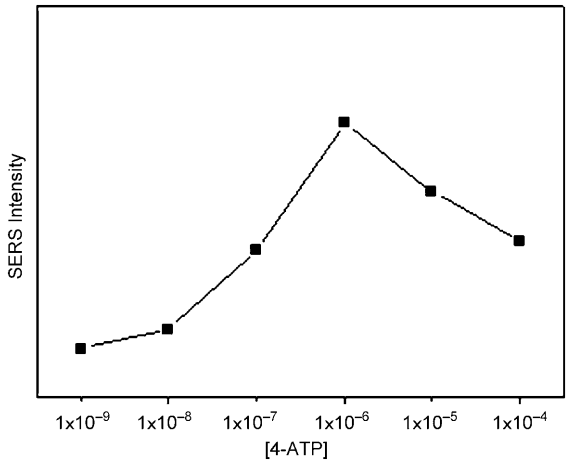

Figure 6. SERS intensity of the TNT marker band at 1359 cm^{-1} at different PATP concentrations.

1359 cm^{-1} at different PATP concentrations is plotted. The feature at 1359 cm^{-1} was selected as the marker band because it appears in a spectral region rather free of DMAB bands and is one of the strongest bands in the TNT spectrum. On increasing the PATP surface coverage, the number of imprint molecular sites available for the TNT π-donor–acceptor interaction complex grows, but the imprint molecular sites simultaneously adopt a closer configuration at higher concentration,[5] which in turn reduces the efficiency of the π-donor–acceptor interaction. Furthermore, the spectral intensity of a very high concentration of PATP is too high, such that the characteristic peak of the object cannot be easily observed. The maximum of the TNT signal appearing at 10^{-6} M PATP in the colloidal suspension likely corresponds to the best compromise between these two opposite effects, that is, maximum coverage with the lower effect of multilayer PATP adsorption.[34]

Figure 7A shows the SERS spectral intensity of TNT interacting with DMAB-modified Ag-SMNs complex (the most intense band at 1359 cm^{-1} for TNT) on changing the

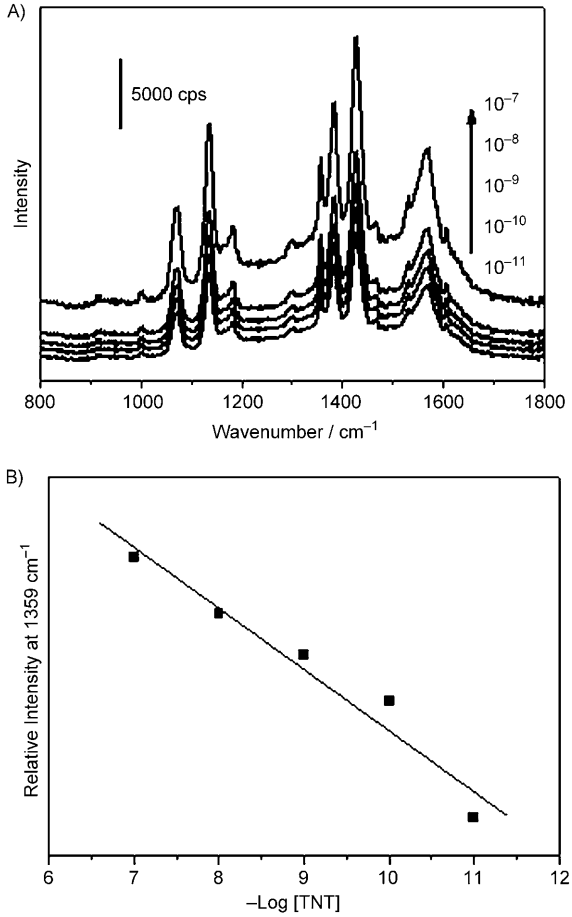

Figure 7. A) SERS spectra obtained for different concentrations of TNT using imprinted DMAB-modified Ag-SMNs complex. [TNT]: from 10^{-7} to 10^{-11} M; [PATP] = 10^{-6} M. B) Logarithmic plot of [TNT] versus SERS intensity together with linear fitting.

TNT concentration, while the PATP concentration was kept constant at 10^{-6} M for all measurements. The TNT concentration was varied from 10^{-7} to 10^{-11} M. The individual spectra shown in Figure 7A each represent the average spectrum that was obtained for the various samples when each was analyzed in five different locations across the spot perimeter using 514.5 nm excitation and an integration time of 10 s. Spectral averaging was carried out to minimize photobleaching and also to minimize the variation in signal intensity. Figure 7B illustrates the corresponding plot of I_{SERS} versus $-\log[TNT]$, in which I_{SERS} is the SERS intensity recorded for the TNT bands at 1359 cm^{-1}. It can be seen that the data can be fitted by a linear plot.

The binding of TNT to the π-donor binding sites in the imprinted Ag-SMNs matrices can be described by Equa-

tion (1). According to this model, the association constant of TNT at the π-donor binding sites is given by Equation (2), in which θ is the number of sites occupied by TNT and α is the total number of binding sites:

$$\begin{array}{c} \text{TNT} + \pi\text{-donor sites} \Leftrightarrow \text{TNT-bound sites} \\ \alpha-\theta \qquad\qquad \theta \end{array} \quad (1)$$

$$K_{ass} = \frac{\theta}{(\alpha-\theta)[\text{TNT}]} \quad (2)$$

which leads to Equation (3)

$$\log(\theta/(\alpha-\theta)) = \log K_{ass} + \log[\text{TNT}] \quad (3)$$

It can be assumed that the only contribution to I_{SERS} of TNT is provided by those TNT molecules interacting with the π-donor binding sites. Thus, $I_{SERS} = C[\alpha/\theta]$, in which the constant C includes all of the physical constants and parameters related to the Raman emission and SERS enhancement that are not related to the concentration of the emitting molecule.[15] This constant can be deduced from the linear graph plotted in Figure 7B. The derived association constant corresponds to $K_{ass} \approx 7.4 \times 10^6\,\text{M}^{-1}$. It should be noted that this method for deriving the association constants assumes that the binding of TNT to the π-donor sites is unaffected by neighboring occupied sites. At the low concentrations of TNT at which the association constant was derived, this assumption is justified. Based on Eq. (3) and Figure 7B, the limit of detection (LOD) is about 10^{-12} M, which is calculated considering the lowest concentration leading to a SERS intensity of the marker band at 1359 cm^{-1} that would produce a signal to noise ratio >2. To the best of our knowledge, the LOD achieved with our SERS probe is one of the lowest among the reported methods.

Kinetics of up-take of the target species: Figure 8 shows the time-dependent evolution of the SERS intensity change rate of TNT bound by non-imprinted DMAB-modified Ag-SMNs complex and imprinted DMAB-modified Ag-SMNs complex. It is well known that the SERS intensity is directly proportional to the adsorbed amount of TNT. Before equilibrium adsorption was reached, the imprinted DMAB-modified Ag-SMNs complex took up TNT molecules from the solution phase at a much faster rate than the non-imprinted DMAB-modified Ag-SMNs complex. The imprinted particles took up 50% of the equilibrium amount in only 10 s, whereas the non-imprinted particles needed 80 s to take up 50% of the equilibrium amount. Figure 8 also reveals a rapid adsorption of TNT molecules onto the imprinted DMAB-modified Ag-SMNs complex. The binding rate of TNT on the imprinted materials obtained from the fitting results is faster than that on the non-imprinted DMAB-modified Ag-SMNs complex. Usually, rapid binding kinetics requires that more recognition sites are situated at the surface or in the proximity of the surface for easy diffusion of the target species to these sites.[24] In our system, imprinted particles have more recognition sites. After about 60 s, the rate of change of SERS intensity of the imprinted particles tends to level off. We concluded that the time interval of 60 s for incubating the functionalized Ag-SMNs complex with the samples was sufficient for generating a SERS signal corresponding to about 90% of the saturation value. In contrast, the equilibrium period for the non-imprinted nanoparticles was estimated to be longer than 400 s (data not shown). Therefore, the imprinted nanoparticles display very fast binding kinetics for the target species. These results clearly suggest that the SERS sensor device may be of potential applicability in real life.

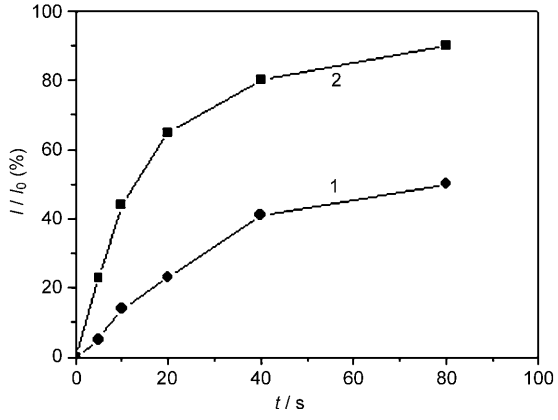

Figure 8. Time-dependent SERS intensity changes upon the analysis of a TNT sample, 1) by the non-imprinted DMAB-modified Ag-SMNs complex, and 2) by the imprinted DMAB-modified Ag-SMNs complex. The binding kinetics data were obtained using a 10^{-6} M TNT solution. I_0 is the peak intensity of the TNT marker band at 1359 cm^{-1}. [PATP] = 10^{-6} M.

Selectivity and sensitivity of SERS response of imprinted SERS substrate: To ascertain whether our assay is highly selective, we also investigated how the SERS intensity changes upon addition of 2,4-dinitrotoluene (DNT). Figure 9 shows the SERS responses of our new probe in the presence of DNT and TNT. Curve a shows no Raman signal from TNT in the Ag-SMNs complex. The peak at 935 cm^{-1} may be attributed to SMNs. The band is related to stretching vibrations of molybdate with fourfold coordination of oxygen atoms around the molybdenum atom.[44] The signals are quite weak compared with those of SERS in Figure 9. Curve b features a very weak spectral peak in the 1333 cm^{-1} region, which corresponds to the characteristic 2,4-DNT NO_2 stretching mode (γNO_2).[45,46] Although the key SERS-enhanced features are qualitatively similar for TNT and DNT, it is possible to uniquely identify each component (see Figure 9B). The SERS nitro stretching modes are observed at 1359 and 1333 cm^{-1} for TNT and 2,4-DNT, respectively.[45] The reproducibility of the positions of these peaks is conservatively estimated to be $\pm 2\,\text{cm}^{-1}$. Curves c and d clearly show the Raman signals from TNT at about 1359, 1532, and 1609 cm^{-1}. It can be seen that the intensity of the TNT signals in the imprinted complex is about fourfold higher than that with the non-imprinted DMAB-modified Ag-SMNs complex. The enhanced sensitivity for analyzing TNT by the

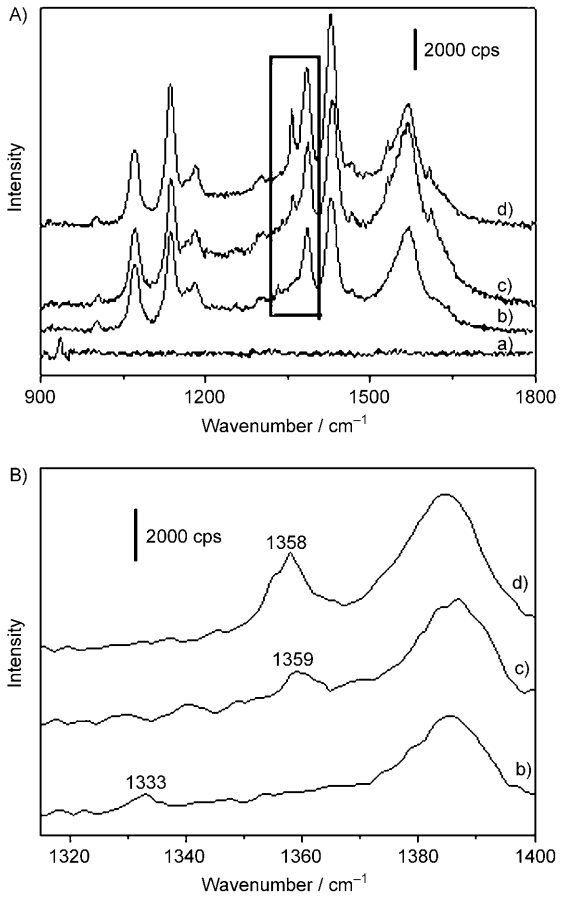

Figure 9. A) SERS spectra of a) TNT + Ag-SMNs complex, b) DNT + imprinted DMAB-modified Ag-SMNs complex, c) TNT + non-imprinted DMAB-modified Ag-SMNs complex, and 4) TNT + imprinted DMAB-modified Ag-SMNs complex. B) Detailed regions from 1315 to 1400 cm^{-1} of A. [TNT] = 1 nM, [DNT] = 10^{-6} M. All data were recorded after allowing the respective substrates to interact with the TNT solution for 60 s.

imprinted complex is attributed to the greater concentration of the analyte at the surface of the Ag nanoparticles as a result of its higher affinity for the imprinted π-donor sites. Removal of the TNT imprint molecules (particle **5** in Scheme 2) yields molecular contours with optimal positioning of the π-donor sites for the association of the TNT analyte. Indeed, in a previous study, it was demonstrated that the synergistic binding of TNT to an imprinted complex through π-donor–acceptor interactions and molecular contours improved the association constant of TNT to the matrix.[22] Thus, the imprinting procedure with TNT not only increases the sensitivity of the modified complex but also impressively enhances its selectivity toward the analysis of TNT. Comparing curves b and d in Figure 9, the results clearly confirm the effectiveness of the molecular imprinting because imprinted DMAB-modified Ag-SMNs complex shows a much higher selectivity for TNT than for DNT, even though the concentration of DNT is 1000 times higher than that of TNT. This is because DNT exhibits lower π-acceptor properties due to the decreased number of electron-withdrawing nitro groups, and hence its concentration at the complex surface anchored through π-donor–acceptor interactions is substantially lower. It is therefore expected that the sensitivity for the detection of the DNT as a substrate will be lower due to the inferior π-acceptor properties of this analyte. These results imply that the selectivity is, indeed, induced by π-donor–acceptor interactions between the different nitroaromatic compounds and the π-donor DMAB bridges.

Conclusion

A new strategy for the ultra-trace detection of TNT is presented using *p*-aminothiophenol-based complexation and SERS on silver nanoparticles attached to silver molybdate nanowires. The limit of detection deduced for this technique is 10^{-12} M. PATP molecules adsorbed on silver nanoparticles undergo a catalytic coupling reaction to produce DMAB, which can form an array of SERS "hot spots". We have shown that π-donor–acceptor interactions between TNT and π-donor DMAB cross-linked silver nanoparticles linked to silver molybdate nanowires, the optimal imprint molecule contours, and SERS "hot spots" at which the analyte can be anchored, provide a significant enhancement of the Raman signal intensity. The results show that TNT can be detected quickly and accurately without any dye tagging. It is evident that molecular recognition sites were successfully imprinted in the modified Ag-SMNs, which has important implications for the future development of sensing devices. Although the current work has been mainly focused on the imprinting of TNT molecules, we have also demonstrated that this imprinting technique is generally applicable to various other organic molecules, such as polycyclic aromatic hydrocarbons. The silver/silver molybdate nanowire complex has been demonstrated to act as a new type of SERS substrate. The results have shown that the imprinted π-donor DMAB-modified Ag NPs array offers a highly sensitive, rapid, easy, and reliable means of detecting TNT in environmental samples by measuring the TNT SERS intensity.

Experimental Section

Materials: Tungstosilicic acid ($H_4(SiW_{12}O_{40})$; TSA]), silver nitrate ($AgNO_3$), sodium molybdate (Na_2MoO_4), and ethanol were all obtained as A.R. grade from Shanghai Reagent Co., and were used without further purification. *p*-Aminothiophenol (PATP) was purchased from Sigma–Aldrich and was used without further purification. 2,4,6-Trinitrotoluene (TNT) was supplied by the National Security Department of China and was recrystallized from ethanol before use. Doubly distilled water was used throughout to prepare the solutions.

Preparation of silver and silver molybdate complex: In a typical experiment, 2-propanol (2 mL) and a deaerated 2 mM solution of tungstosilicic acid in water (30 mL) were added to a deaerated 4 mM solution of $AgNO_3$ in water (15 mL). Subsequently, a 4 mM solution of Na_2MoO_4 in water (15 mL) was added with continuous stirring over 30 min, and then the mixture was set aside for 2 h at room temperature. A homogeneous light-yellow solution was formed, indicating the formation of silver molybdate. Irradiation of the above mixture with UV light (Pyrex filter,

>280 nm, 450 W Hanovia medium-pressure lamp) for 2 h resulted in a gradual color change to gray, thus indicating the formation of the silver and silver molybdate complex. Details of the reaction mechanism are provided in our former publications.[27,28] The complex was collected by filtration, washed several times with doubly distilled water, and dried in a vacuum oven at 60°C for 6 h. The concentration of Ag NPs was measured by UV/Vis spectroscopy using the molar extinction coefficient at the wavelength of maximum absorption of Ag colloid.

Silver nanoparticle surface modification: To enable the selective detection of TNT, we modified the surface of the silver nanoparticles with PATP. Freshly prepared Ag-SMNs complex (the original concentration of silver molybdate complex was 10^{-5} M) and PATP (10^{-6} M) were mixed in a 9:1 volume ratio and stirred for 10 h. Excess PATP was removed by centrifugation at 5000 rpm for several minutes.

Imprinting of TNT recognition sites: TNT-imprinted DMAB films were prepared by adding 1 mM TNT to the PATP-modified Ag-SMNs complex prior to the irradiation process. PATP and DMAB were used as the functional monomer and cross-linking agent for the photonic catalytic coupling imprinting process, respectively. TNT template molecules in the imprinted DMAB-modified Ag-SMNs complex were removed by three extractions with 9:1 (v/v) CH_3OH/HOAc, each performed for 2 h at room temperature under continuous agitation. The product, having a high density of cross-linking imprint sites, was then separated from the mixed solution by centrifugation. The amount of TNT bound to the imprinted particles was determined by measuring the difference between the total amount of TNT and the residual amount in the solution. Meanwhile, the binding kinetics was tested by monitoring the temporal evolution of the TNT concentration in the solution containing the imprinted materials. The binding rates of the imprinted particles to the target analyte were obtained by fitting the time-dependent amount of TNT molecules taken up. The molecular recognition selectivity of the imprinted particles was investigated by using structurally analogous DNT as a substrate to compete with TNT. For comparison, the same measurements were also carried out with non-imprinted particles.

Characterization: UV/Vis absorbance spectra were measured with a UNIC UV-4802 spectrometer. XRD analysis was carried out with an MAP18AHF instrument (Japan MAC Science Co.). The morphologies and structures of the nanoparticles were examined by means of an FEI Sirion-200 field-emission scanning electron microscope and a JEOL 2010 transmission electron microscope. TNT was quantitatively analyzed by means of a Waters Module-600 high-performance liquid chromatograph with UV 996 detector. Macro-SERS spectra were recorded with a Renishaw Raman RM2000 spectrometer equipped with a 514.5 nm laser, an electrically refrigerated CCD camera, and a notch filter to eliminate the elastic scattering. The spectra shown here were obtained by using a lens of 30 mm focus length. The output laser power on the sample was about 2 mW. Spectral resolution was 4 cm^{-1}. These spectral scanning conditions were chosen to avoid sample degradation. The reported spectra were registered as single scans.

Acknowledgements

The financial support of this work by the National Basic Research Program of China (2007CB936603 and 2009CB939902), a China Postdoctoral Science Foundation funded project (20070420739), the Hi-tech Research and Development Program of China (863 Program) (2009AA03Z330), and the National Natural Science Foundation of China (grant no. 10635070) is gratefully acknowledged.

[1] K. N. Houk, G. L. Leach, S. P. Kim, X. Zhang, *Angew. Chem.* **2003**, *115*, 5020–5046; *Angew. Chem. Int. Ed.* **2003**, *42*, 4872–4897.
[2] P. Leyton, C. Domingo, S. Sanchez-Cortes, M. Campos-Vallette, G. F. Diaz, J. V. Garcia-Ramos, *Vib. Spectrosc.* **2007**, *43*, 358–365.
[3] P. Morf, F. Raimondi, H. G. Nothofer, B. Schnyder, A. Yasuda, J. M. Wessels, T. A. Jung, *Langmuir* **2006**, *22*, 658–663.
[4] L. Guerrini, J. V. Garcia-Ramos, C. Domingo, S. Sanchez-Cortes, *Langmuir* **2006**, *22*, 10924–10926.
[5] L. Guerrini, J. V. Garcia-Ramos, C. Domingo, S. Sanchez-Cortes, *Anal. Chem.* **2009**, *81*, 953–960.
[6] L. Guerrini, J. V. Garcia-Ramos, C. Domingo, S. Sanchez-Cortes, *Phys. Chem. Chem. Phys.* **2009**, *11*, 1787–1793.
[7] A. Miyawaki, M. Miyauchi, Y. Takashima, H. Yamaguchi, A. Harada, *Chem. Commun.* **2008**, 456–458.
[8] M. W. J. Beulen, J. Bugler, M. R. de Jong, B. Lammerink, J. Huskens, H. Schonherr, G. J. Vancso, B. A. Boukamp, H. Wieder, A. Offenhauser, W. Knoll, F. C. J. M. van Veggel, D. N. Reinhoudt, *Chem. Eur. J.* **2000**, *6*, 1176–1183.
[9] P. Kuad, A. Miyawaki, Y. Takashima, H. Yamaguchi, A. Harada, *J. Am. Chem. Soc.* **2007**, *129*, 12630–12631.
[10] A. McNally, R. J. Forster, T. E. Keyes, *Phys. Chem. Chem. Phys.* **2009**, *11*, 848–856.
[11] A. D. Strickland, C. A. Batt, *Anal. Chem.* **2009**, *81*, 2895–2903.
[12] P. M. S. Monk, *The Viologens: Physicochemical Properties, Synthesis and Applications of the Salts of 4,4′-Bipyridine*, Wiley, New York, **1998**.
[13] L. Guerrini, J. V. Garcia-Ramos, C. Domingo, S. Sanchez-Cortes, *J. Phys. Chem. C.* **2008**, *112*, 7527–7530.
[14] L. Guerrini, J. V. Garcia-Ramos, C. Domingo, S. Sanchez-Cortes, *Anal. Chem.* **2009**, *81*, 1418–1425.
[15] L. Guerrini, A. E. Aliaga, J. Carcamo, J. S. Gomez-Jeria, S. Sanchez-Cortes, M. M. Campos-Vallette, J. V. Garcia-Ramos, *Anal. Chim. Acta* **2008**, *624*, 286–293.
[16] K. D. Smith, B. R. McCord, W. A. MacCrehan, K. Mount, W. F. Rowe, *J. Forensic Sci.* **1999**, *44*, 789–794.
[17] P. T. Charles, B. M. Dingle, S. Van Bergen, P. R. Gauger, C. H. Patterson, A. W. Kusterbeck, *Field Anal. Chem. Technol.* **2001**, *5*, 272–280.
[18] J. Hawari, S. Beaudet, A. Halasz, S. Thiboutot, G. Ampleman, *Appl. Microbiol. Biotechnol.* **2000**, *54*, 605–618.
[19] T. M. Swager, *Acc. Chem. Res.* **1998**, *31*, 201–207.
[20] D. T. McQuade, A. E. Pullen, T. M. Swager, *Chem. Rev.* **2000**, *100*, 2537–2574.
[21] S. S. R. Dasary, A. K. Singh, D. Senapati, H. T. Yu, P. C. Ray, *J. Am. Chem. Soc.* **2009**, *131*, 13806–13812.
[22] M. Riskin, R. Tel-Vered, T. Bourenko, E. Granot, I. Willner, *J. Am. Chem. Soc.* **2008**, *130*, 9726–9733.
[23] M. Riskin, R. Tel-Vered, O. Lioubashevski, I. Willner, *J. Am. Chem. Soc.* **2009**, *131*, 7368–7378.
[24] C. G. Xie, Z. P. Zhang, D. P. Wang, G. J. Guan, D. M. Gao, J. H. Liu, *Anal. Chem.* **2006**, *78*, 8339–8346.
[25] C. G. Xie, B. H. Liu, Z. Y. Wang, D. M. Gao, G. J. Guan, Z. P. Zhang, *Anal. Chem.* **2008**, *80*, 437–443.
[26] D. M. Gao, Z. P. Zhang, M. H. Wu, C. G. Xie, G. J. Guan, D. Y. Wang, *J. Am. Chem. Soc.* **2007**, *129*, 7859–7866.
[27] L. B. Yang, Y. H. Shen, A. J. Xie, J. J. Liang, J. M. Zhu, L. Chen, *Eur. J. Inorg. Chem.* **2007**, 1128–1134.
[28] L. B. Yang, Y. H. Shen, A. J. Xie, B. C. Zhang, *J. Phys. Chem. C.* **2007**, *111*, 5300–5308.
[29] N. R. Walker, M. J. Linman, M. M. Timmers, S. L. Dean, C. M. Burkett, J. A. Lloyd, J. D. Keelor, B. M. Baughman, P. L. Edmiston, *Anal. Chim. Acta* **2007**, *593*, 82–91.
[30] R. K. R. Jetti, R. Boese, T. S. Thakur, V. R. Vangala, G. R. Desiraju, *Chem. Commun.* **2004**, 2526–2527.
[31] A. Grirrane, A. Corma, H. Garcia, *Science* **2008**, *322*, 1661–1664.
[32] Y. Matsuda, A. Shono, C. Iwakura, Y. Ohshiro, T. Agawa, H. Tamura, *Bull. Chem. Soc. Jpn.* **1971**, *44*, 2960–2963.
[33] E. Roth, C. Engert, W. Kiefer, *J. Mol. Struct.* **1995**, *349*, 89–92.
[34] H. K. Park, S. B. Lee, K. Kim, M. S. Kim, *J. Phys. Chem.* **1990**, *94*, 7576–7580.
[35] P. Gao, D. Gosztola, M. J. Weaver, *J. Phys. Chem.* **1989**, *93*, 3753–3760.
[36] D. Y. Wu, X. M. Liu, Y. F. Huang, B. Ren, X. Xu, Z. Q. Tian, *J. Phys. Chem. A* **2009**, *113*, 18212–18222.
[37] W. Hill, B. Wehling, *J. Phys. Chem.* **1993**, *97*, 9451–9455.

[38] M. Osawa, N. Matsuda, K. Yoshii, I. Uchida, *J. Phys. Chem.* **1994**, *98*, 12702–12707.
[39] Q. Zhou, X. W. Li, Q. Fan, X. X. Zhang, J. W. Zheng, *Angew. Chem.* **2006**, *118*, 4074–4077; *Angew. Chem. Int. Ed.* **2006**, *45*, 3970–3973.
[40] A. Ashkin, *Phys. Rev. Lett.* **1970**, *24*, 156–159.
[41] D. G. Grier, *Nature* **2003**, *424*, 810–816.
[42] M. W. Shao, L. Lu, H. Wang, S. Wang, M. L. Zhang, D. D. D. Ma, S. T. Lee, *Chem. Commun.* **2008**, 2310–2312.
[43] M. V. Cañamares, J. V. Garcia-Ramos, J. D. Gomez-Varga, C. Domingo, S. Sanchez-Cortes, *Langmuir* **2007**, *23*, 5210–5215.
[44] R. Lewandowska, K. Krasowski, R. Bacewicz, J. E. Garbarczyk, *Solid State Ionics* **1999**, *119*, 229–234.
[45] J. M. Sylvia, J. A. Janni, J. D. Klein, K. M. Spencer, *Anal. Chem.* **2000**, *72*, 5834–5840.
[46] H. Ko, V. V. Tsukruk, *Small* **2008**, *4*, 1980–1984.

Received: April 21, 2010
Published online: September 17, 2010

